Mon. Not. R. Astron. Soc. **356,** 183–191 (2005) doi:10.1111/j.1365-2966.2004.08432.x

The *XMM–Newton*/2dF Survey – VI. Clustering and bias of the soft X-ray point sources

S. Basilakos,[1⋆] M. Plionis,[1,2] A. Georgakakis[1] and I. Georgantopoulos[1]

[1]*Institute of Astronomy & Astrophysics, National Observatory of Athens, I. Metaxa & V. Pavlou, Palaia Penteli, 15236 Athens, Greece*
[2]*Instituto Nacional de Astrofisica, Optica y Electronica (INAOE) Apartado Postal 51 y 216, 72000 Puebla, Pue., Mexico*

Accepted 2004 September 22. Received 2004 August 27; in original form 2004 June 9

ABSTRACT

We study the clustering properties of X-ray sources detected in the wide area ($\sim$2 deg^2) bright, contiguous *XMM–Newton*/2dF survey. We detect 432 objects to a flux limit of 5×10^{-15} erg cm^{-2} s^{-1} in the soft 0.5–2 keV band. Performing the standard angular correlation function analysis, a $\sim 3\sigma$ correlation signal between 0 and 150 arcsec is detected: $w(\theta < 150\,\mathrm{arcsec}) \simeq 0.114 \pm 0.037$. If the angular correlation function is modelled as a power law, $w(\theta) = (\theta_0/\theta)^{\gamma-1}$, then for its nominal slope of $\gamma = 1.8$ we estimate, after correcting for the integral constraint and the amplification bias, that $\theta_0 \simeq 10.4 \pm 1.9$ arcsec. Very similar results are obtained for the 462 sources detected in the total 0.5–8 keV band ($\theta_0 \simeq 10.8 \pm 1.9$ arcsec).

Using a clustering evolution model which is constant for comoving coordinates ($\epsilon = -1.2$), a luminosity-dependent density evolution (LDDE) model for the X-ray luminosity function and the concordance cosmological model ($\Omega_\mathrm{m} = 1 - \Omega_\Lambda = 0.3$) we obtain, by inverting Limber's integral equation, a spatial correlation length of $r_0 \sim 16\,h^{-1}$ Mpc. This value is larger than that of previous *ROSAT* surveys as well as of the optical two-degree quasar redshift survey. Only in models where the clustering remains constant for physical coordinates ($\epsilon = -3$), do we obtain an r_0 value ($\sim 7.5\,h^{-1}$ Mpc) which is consistent with the above surveys.

Finally, comparing the measured angular correlation function with the predictions of the concordance cosmological model, we find for two different bias evolution models that the soft X-ray sources at the present time should be biased with respect to the underline matter fluctuation field with bias values in the range (which depends on the biasing model used): $1.9 \lesssim b_0 \lesssim 2.7$ for $\epsilon = -1.2$ or $1 \lesssim b_0 \lesssim 1.6$ for $\epsilon = -3$.

Key words: galaxies: clusters: general – cosmology: theory – large-scale structure of Universe.

1 INTRODUCTION

Active galactic nuclei (AGN) can be detected out to high redshifts and therefore, study of their clustering properties can provide information on both the large-scale structure of the underlying matter distribution and its evolution with redshift. At optical wavelengths the 2 degree field quasi-stellar object redshift survey (2QZ; Croom et al. 2002) comprising over 25 000 optically selected QSOs in the range $z \approx 0.3$–3 has provided tight constraints on the spatial distribution of powerful AGN (Croom, Shanks & Boyle 2001; Croom et al. 2002). A striking result from this survey was that the clustering properties of QSOs are comparable to those of local galaxies. Moreover, when studied as a function of redshift the clustering of these sources was found to be constant up to $z \approx 3$.

Optically selected AGN catalogues, however, are believed to miss large numbers of dusty systems and therefore, provide a biased census of the AGN phenomenon. X-ray surveys, are least affected by dust providing an efficient tool for compiling uncensored AGN samples over a wide redshift range. From a cosmological point of view an interesting question that remains to be addressed is how the X-ray selected AGN trace the underlying mass distribution and whether there are any differences with optically selected samples. Despite the importance of X-ray selected AGN, their clustering properties remain poorly constrained. Early studies with the *Einstein* and *ROSAT* satellites have produced contradictory results. Boyle & Mo (1993) used low-redshift AGN detected in the Einstein Medium Sensitivity Survey Einstein Medium Sensitivity Survey (reference) and found only a marginally significant clustering signal at scales <10 h^{-1} Mpc. Vikhlinin & Forman (1995) combined archival *ROSAT* observations totaling 40 deg^2 and detected, for the first time, a statistically significant clustering signal using angular correlation function analysis. Their results suggest a clustering length consistent with that of optically selected QSOs. Akylas, Georgantopoulos & Plionis (2000) used the *ROSAT* All Sky Survey Bright Source Catalogue to explore the clustering of nearby AGN. They estimate

⋆E-mail: svasil@astro.noa.gr

$r_0 = 6.5 \pm 1.0\ h^{-1}$ Mpc, which is also similar to nearby galaxies and the 2QZ survey results. Contrary to the studies above that are based on an angular correlation analysis, Carrera et al. (1998) used redshift information to measure the spatial correlation function of X-ray sources in the *ROSAT* Deep (Georgantopoulos et al. 1996) and RIXOS (Mason et al. 2000) surveys. They detect only a marginally significant clustering signal and argue that their results suggest that the X-ray population is more weakly clustered than optically selected galaxies or AGN. Recently, Mullis et al. (2004) using the *ROSAT* North Ecliptic Pole survey of relatively local X-ray selected AGN, found a spatial correlation length of $r_0 \simeq 7.4 \pm 1.8\ h^{-1}$ Mpc within the concordance cosmological model.

The new generation *Chandra* and *XMM–Newton* telescopes have extended the studies above to the hard (2–8 keV) spectral band. Yang et al. (2003) used *Chandra* observations and argued that hard (2–8 keV) X-ray selected sources have large variance (strong clustering) and are most likely associated with high-density regions. These authors also find that X-ray sources selected in the soft (0.5–2 keV) energy band are less clustered (about 1 dex) than hard ones. Recently, Basilakos et al. (2004) applied an angular correlation function analysis to hard X-ray selected sources detected in the wide area, shallow *XMM–Newton*/2dF survey. They find a strong signal consistent with a spatial clustering length in the range $r_0 \sim 10$–$19\,h^{-1}$ Mpc (in the concordance cosmological model). This also suggests that hard X-ray sources could trace the high-density peaks of the underlying mass distribution.

In this paper we further explore the clustering properties of the X-ray population exploiting the high sensitivity and the large field-of-view of the *XMM–Newton* observatory. In particular, we extend the Basilakos et al. (2004) clustering study to sources detected in the soft (0.5–2 keV) and the total (0.5–8 keV) spectral bands of a wide area ($\approx 2\,\mathrm{deg}^2$), contiguous *XMM–Newton* survey (*XMM–Newton*/2dF survey). Our study provides the first constraints on the clustering properties of the sources in the above spectral bands using the *XMM–Newton*. Furthermore, we model our X-ray source clustering and its evolution in an attempt to derive their present time bias with respect to the underline mass fluctuation field.

The structure of the paper is as follows. The X-ray sample is presented in Section 2 and the angular correlation function analysis is discussed in Section 3, while the spatial clustering predictions are presented in Section 4. Section 5 outlines the models used to interpret the angular correlation function results and the theoretical interpretation of the X-ray source clustering. Finally, we draw our conclusions in Section 6. Hereafter and wherever necessary we will assume the *concordance* cosmological model (unless stated otherwise), i.e. $\Omega_{\rm m} + \Omega_\Lambda = 1$, $\Omega_{\rm m} = 0.3$, $H_0 = 100\ h$ km s^{-1} Mpc^{-1} (Spergel et al. 2003; Tegmark et al. 2004) with $h \simeq 0.7$ (Freedman et al. 2001; Peebles & Ratra 2003; and references therein) and baryonic density parameter $\Omega_{\rm b}h^2 \simeq 0.02$ (cf. Olive, Steigman & Walker 2000; Kirkman et al. 2003).

2 THE SAMPLE

The X-ray data used in this study are from the *XMM–Newton*/2dF survey. This is a shallow (2–10 ks per pointing) survey carried out by the *XMM–Newton* near the North Galactic Pole [NGP; RA(J2000) = $13^{\rm h}41^{\rm m}$; Dec.(J2000) = $00^\circ00'$] and the South Galactic Pole [SGP; RA(J2000) = $00^{\rm h}57^{\rm m}$, Dec.(J2000) = $-28^\circ00'$] regions. A total of 18 *XMM–Newton* pointings were observed equally split between the NGP and the SGP areas. A number of pointings were discarded owing to an elevated particle background at the time of the observation resulting in a total of 13 usable *XMM–Newton* pointings. A full description of the data reduction, source detection and flux estimation are presented by Georgakakis et al. (2003, 2004).

Here we use the soft (0.5–2 keV) and the total (0.5–8 keV) band catalogues of the *XMM–Newton*/2dF survey. We only consider sources at off-axis angles <13.5 arcmin. The two samples comprise 432 and 462 sources, respectively, above the 5σ detection threshold. The limiting fluxes are $f_X(0.5\text{–}2) = 2.7 \times 10^{-15}$ erg s^{-1} cm^{-2} and $f_X(0.5\text{–}8) = 6.0 \times 10^{-15}$ erg s^{-1} cm^{-2}. The sensitivity of the *XMM–Newton* degrades from the centre to the edge of the field of view (vignetting) and therefore the limiting flux varies across the surveyed area. We account for this effect by constructing sensitivity maps giving the area of the survey accessible to point sources above a given flux limit. In the 0.5–8 keV band about 10 per cent of the surveyed area is covered at the flux $f_X(0.5\text{–}8\ \mathrm{keV}) = 10^{-14}$ erg s^{-1} cm^{-2}. This fraction increases to about 50 per cent at $f_X(0.5\text{–}8\ \mathrm{keV}) = 2 \times 10^{-14}$ erg s^{-1} cm^{-2}. In the soft band about 10 and 50 per cent of the total area is covered at the flux $f_X(0.5\text{–}2\ \mathrm{keV}) = 3.5 \times 10^{-15}$ and 5×10^{-15} erg s^{-1} cm^{-2}, respectively.

Unfortunately, the identification of our sources in the 0.5–2 keV band remains largely unknown because optical spectroscopy is not available for most of them. However, from other surveys in the same band and of similar depth, we know that most sources are associated with AGN. For example, among the 50 soft X-ray selected sources in the *ROSAT* Lockman Deep Field (Schmidt et al. 1998), reaching a flux depth of $f_{0.5\text{–}2} \approx 10^{-15}$ erg cm^{-2} s^{-1}, 65 and 15 per cent are broad-line and narrow-line AGN, respectively. A small contamination (6 per cent) by stars is also expected (Schmidt et al. 1998), but as they are randomly distributed over the sky their effect would be to dilute somewhat the measured correlation signal. From the work of Woods & Fahlman (1997) we can deduce that for a stellar contamination of 6 per cent a reduction in the observed correlation signal by $\sim$13 per cent should be expected (correcting for this reduces our r_0 values, derived in Section 4 by only $\sim$5 per cent). In the *ROSAT* Lockman Hole Survey there is also a small fraction of galaxy groups. As these may be more strongly clustered than galaxies, and possibly AGN, they may increase marginally the overall signal. For this reason we have excluded the nine extended sources, which we have found in our *XMM* observations, from the subsequent analysis.

The differential X-ray source counts in the 0.5–2 and 0.5–8 keV spectral bands are shown in Fig. 1 and are compared with the best-fitting relations of Baldi et al. (2002, soft band) and Manners et al. (2003; total band). In the 0.5–2 keV band there is good agreement between our results and the Baldi et al. (2002) double power-law best-fitting relation to the number counts. The best-fitting relation of Manners et al. (2003) is derived for sources in the flux range $f(0.5\text{–}8\,\mathrm{keV}) = 10^{-15}$–$8 \times 10^{-14}$ erg s^{-1} cm^{-2}. Although our $\mathrm{d}N/\mathrm{d}S$ is in good agreement with their results in the above flux range, at brighter fluxes the surface density of X-ray sources is lower than the extrapolated Manners et al. (2003) relation. This suggests that a double power law is required to fit the 0.5–8 keV $\mathrm{d}N/\mathrm{d}S$ over the flux range 10^{-15} –10^{-12} erg s^{-1} cm^{-2}. We therefore adopt a double power law of the form

$$\log \frac{\mathrm{d}N}{\mathrm{d}S} = \begin{cases} A_1 + B_1 \times \log f_X & f_X < f_X^c \\ A_2 + B_2 \times \log f_X & f_X \geqslant f_X^c \end{cases},$$

where $A_2 = A_1 + (B_1 - B_2) \times f_X^c$ with f_X^c being the flux at the break. We estimate $f_X^c(0.5\text{–}8\ \mathrm{keV}) \approx 6 \times 10^{-14}$ erg s^{-1} cm^{-2}, $A_1 = -8.9 \pm 2.2$, $B_1 = -1.8 \pm 0.2$ and $B_2 = -2.3 \pm 0.1$. Our best-fitting double power-law relation is shown in Fig. 1.

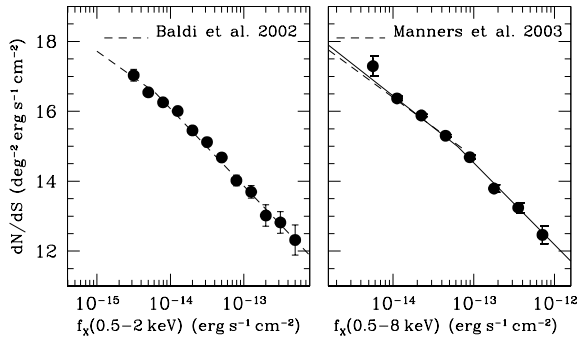

Figure 1. Left-hand panel: the soft band 0.5–2 keV differential number counts from the present survey in comparison with the best-fitting double power law to the counts from Baldi et al. (2002, dashed line). Right-hand panel: the total band (0.5–8 keV) differential counts from the present survey in comparison with the results from Manners et al. (2003; dashed line) spanning the flux range 10^{-15} –8×10^{-14} erg s^{-1} cm^{-2}. At bright fluxes extrapolation of the best-fitting relation of Manners et al. (2003) overestimates the observed X-ray source surface density. The continuous line is our best-fitting relation to the 0.5–8 keV counts from the *XMM–Newton*/2dF survey using the double power law described in the text.

3 TWO-POINT CORRELATION FUNCTION ANALYSIS

The two-point angular correlation function, $w(\theta)$, is defined as the joint probability of finding sources separated by an angle θ. For a random distribution of sources $w(\theta) = 0$ and, therefore, the angular correlation function provides a measure of galaxy density excess over that expected for a random distribution. In this paper we use the estimator described by Efstathiou et al. (1991)

$$w(\theta) = f\frac{N_{\rm DD}}{N_{\rm DR}} - 1, \tag{1}$$

with the uncertainty in $w(\theta)$ being estimated from the relation

$$\sigma_w = \sqrt{(1 + w(\theta))/N_{\rm DR}}, \tag{2}$$

where $N_{\rm DD}$ being the number of data–data pairs in the interval $[\theta - \Delta\theta, \theta + \Delta\theta]$ and $N_{\rm DR}$ is the number of data–random pairs for a given separation. In the above relation f is the normalization factor $f = 2\,N_{\rm R}/(N_{\rm D} - 1)$ with $N_{\rm D}$ and $N_{\rm R}$ being the total number of data and random points, respectively. For each *XMM* pointing we produce 100 Monte Carlo random catalogues having the same number of points as the real data which also account for the sensitivity variations across the surveyed area (see Section 2). Furthermore, as the flux threshold for source detection depends on the off-axis angle from the centre of each of the *XMM–Newton* pointing, the sensitivity maps are used to discard random points in less sensitive areas. This is accomplished by assigning a flux to each random point using the differential source counts plotted in Fig. 1. If that flux is less than five times the local rms noise at the position of the random point (assuming Poisson statistics for the background) this is excluded from the random data set. We have verified that our random simulations reproduce both the off-axis sensitivity of the detector and the individual field $\log N - \log S$. Using the methods described above we estimate $w(\theta)$ in logarithmic intervals with $\delta \log\theta \simeq 0.05$. For both samples we estimate $w(\theta < 150\,\text{arcsec}) \simeq 0.11 \pm 0.03$ corresponding to a statistically significant signal at the $\approx 3.5\sigma$ confidence level (Poisson statistics). We now fit the measured correlation function assuming a power law of the form $w(\theta) = (\theta_0/\theta)^{\gamma-1}$, fixing γ to 1.8. We use a standard χ^2 minimization procedure

$$\chi^2(\theta_0) = \sum_{i=1}^{n}\left[\frac{w_{\rm XMM}(\theta^i) - (\theta_0/\theta^i)^{\gamma-1}}{\sigma^i}\right]^2 \tag{3}$$

with each point weighted by its error (σ^i). Note, that the fitting is performed for angular separations in the range 40–1000 arcsec. We also note that our results are insensitive to both the upper cut-off limit in θ and the angular binning (for more than 10 bins) used to estimate $w(\theta)$. Thus, the best-fitting parameters for both the soft and the total band subsamples are: $\theta_0 = 9.3 \pm 1.9$ and $\theta_0 = 9.0 \pm 1.7$ arcsec, respectively. Note that the errors correspond to 1σ ($\Delta\chi^2 = 1.00$) uncertainties, which are estimated using the variation of $\Delta\chi^2 = \chi^2(\theta_0) - \chi^2_{\rm min}(\theta_0)$ ($\chi^2_{\rm min}$ is the absolute minimum value of the χ^2). However, these raw values should be corrected for two possible bias presented below.

3.1 Integral constraint

When calculating the angular correlation function from a bounded region of solid angle Ω, corresponding to the area of the observed field, the background projected local density of sources is N_s/Ω (where N_s is the number of objects brighter than a given flux limit). However, this is an overestimation of the true underlying mean surface density, because of the positive correlation between galaxies at small separations, balanced by negative values of $w(\theta)$ at larger separations. This bias, known as the integral constraint, has the effect of reducing the amplitude of the correlation function by

$$\omega_\Omega = \frac{1}{\Omega^2}\iint w(\theta)\,{\rm d}\Omega_1\,{\rm d}\Omega_2. \tag{4}$$

Clearly, evaluating ω_Ω necessitates a priori knowledge of the angular correlation function. A tentative value of ω_Ω using a range of $w(\theta)$ by varying within 1σ our results is $\omega_\Omega \simeq 0.01$.

Adding ω_Ω to each bin of our raw $w(\theta)$ the integral constraint has a small but not negligible effect on the estimated correlation lengths. Indeed, for the 0.5–2 keV band repeating the fittings using $\omega_\Omega \simeq 0.01$ we find $\theta_0 \simeq 10.7 \pm 1.9$ arcsec and $\theta_0 \simeq 11.1 \pm 1.7$ arcsec for the soft and the total band, respectively.

3.2 Amplification bias

Another bias that may affect the measured angular correlation function of our X-ray sources is the *amplification bias* (e.g. Vikhlinin & Forman 1995). The original quantification of this effect can be traced back to the work of Kaiser (1984) which showed that smoothing of the galaxy distribution using a Gaussian kernel with size similar or larger to the correlation length of the underlying galaxy distribution increases the correlation function of the resulting density peaks compared to that of the underlying galaxies. Furthermore, the larger the smoothing radius the higher the amplitude of the correlation function of the resulting density peaks.

In the present analysis we are faced with a similar situation as the point spread function (PSF) full width half maximum (FWHM) of the *XMM–Newton* detector is of the same order of magnitude ($\sim$6 arcsec) with the measured angular correlation length ($\theta_o \sim 11$ arcsec). X-ray sources separated by less than $\sim$6 arcsec will be observed as a single object. This is in effect a smoothing process, similar to that of the study of Kaiser, with smoothing radius roughly equal to the *XMM–Newton* PSF size. Vikhlinin & Forman (1995) studied the clustering properties of X-ray sources detected on *ROSAT* archival data and found that their measured $w(\theta)$ value

was severely affected by the amplification bias owing to the large FWHM of the *ROSAT* PSF. In our case we expect significantly less problems as the *XMM–Newton* PSF size is smaller than that of the *ROSAT* detector.

We quantify this effect using an approach that is similar to that of Vikhlinin & Forman (1995). These authors used the Soneira & Peebles (1978) algorithm to construct correlated point processes with a variety of in-built correlation amplitudes. Then, using a smoothing window with the size of the *ROSAT* PSF they were able to determine that their measured $w(\theta)$ was artificially enhanced by a factor of $\sim$2.85.

Our method is based on the concept that the galaxy correlation function owing to its power-law nature could be considered a fractal. Therefore one can shift the amplitude of $w(\theta)$ at different scales keeping its slope fixed. This simplifies our study as we do not need to construct different correlated point process with a particular correlation length. Any correlated point processes that are described by a power law with the required exponent can be scaled to have the specific correlation length one requires. For our study we use the publicly available ΛCDM Hubble volume cluster distribution which has a well-defined power-law correlation function with an exponent $\gamma \simeq 1.8$ (Frenk et al. 2000).

Let's assume that the angular correlation function of the model catalogue above has a correlation length $\theta_{o,c}$ while, the true (unaffected from the amplification bias) correlation length of the X-ray point sources is $\theta_{o,x}$. We can translate the angular scale of the model correlation function to that of the *XMM* correlations by multiplying the former scale by the factor

$$f = \theta_{o,x}/\theta_{o,c}.$$

We can now simulate the effect of *XMM* PSF smoothing on the scaled model correlation function by merging all the model pairs with separations less than the PSF FWHM (i.e. $\sim$6 arcsec for the *XMM–Newton*) and then fitting the model angular correlation function to obtain the best-fitting angular correlation length-scale and compare it to that of the *XMM* point source data.

However, as we do not know the value of $\theta_{o,x}$ but it is rather the value that we seek to find from our analysis, we apply an iterative procedure by which we change the value of $\theta_{o,x}$, and thus of f, until the resulting scaled model correlation function (i.e. after smoothing) has an angular correlation length equal to that of the raw *XMM* point source correlations.

The previous analysis shows that our *XMM–Newton* observations are only marginally affected by the amplification bias. The true underlying angular correlation length of the X-ray population is overestimated by $\sim$3–4 per cent. Therefore, we conclude that the corrected (free of the amplification bias) correlation length of the *XMM–Newton* soft X-ray sources is about $\theta_o \simeq 10.4$ arcsec.

We validate the above procedure by recalculating the amplification bias for the case of *ROSAT* observations. We adopt a correlation length (free from amplification bias) of $\theta_{o,x} = 4$ arcsec (Vikhlinin & Forman 1995) and an effective smoothing scale of $\sim$20 arcsec similar to the *ROSAT* PSF FWHM. Our procedure gives that the expected amplified correlation length of the *ROSAT* sources is $\sim$10.5 arcsec a factor of $\sim$2.7 higher than the true value, in excellent agreement with the Vikhlinin & Forman (1995) analysis. We are therefore confident that our method and results are robust.

3.3 The final angular correlation length

After taking into account the corrections described above, we present the corrected angular correlations in Fig. 2 for the soft and total spectral bands. The best-fitting parameters for both subsamples are presented in Table 1.

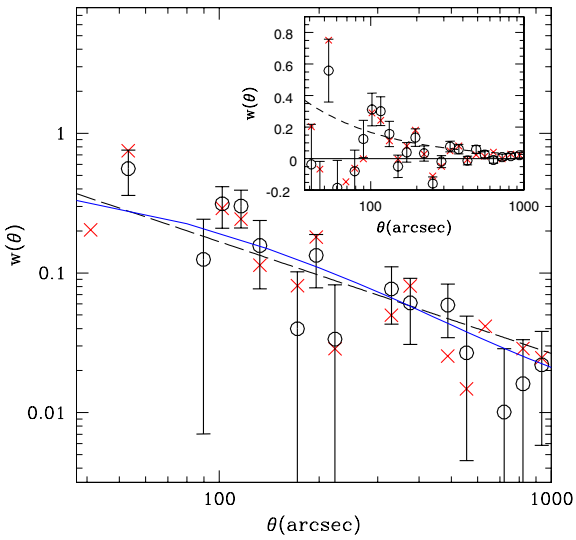

Figure 2. The two-point angular correlation function for the soft (open points) and total (crosses) bands, respectively. The dashed line represent the best-fitting power law $w(\theta) = (\theta_0/\theta)^{0.8}$ for the soft 0.5–2 keV band (see parameters in Table 1), while the continuous line represents the best-fitting ΛCDM ($\Omega_\Lambda = 0.7$ and $h = 0.7$) model in the framework of the Basilakos & Plionis (2001) biasing model. In the insert we present the measured correlation function in linear scaling.

Our results are higher than those of Vikhlinin & Forman (1995) who derive the angular correlation function from *ROSAT* pointed observations which have a comparable effective flux limit with our *XMM* pointings. The above authors find an angular clustering length of $\theta_o \sim 10$ arcsec, which reduces to 4 arcsec after correction for the amplification bias. Comparison with the results of Basilakos et al. (2004) shows that the hard band sources are more strongly clustered, at least on angular projection, ($\theta_0^{\rm hard} \simeq 22 \pm 9$ for $\gamma = 1.8$) compared to the soft band sources.

4 THE SPATIAL CORRELATION LENGTH OF THE *XMM* SOFT SOURCES

4.1 Inverting Limber's equation

The spatial correlation function can be modelled as (de Zotti et al. 1990)

$$\xi(r, z) = (r/r_0)^{-\gamma} \times (1+z)^{-(3+\epsilon)}, \quad (5)$$

where ϵ parametrizes the type of clustering evolution. If $\epsilon = \gamma - 3$ (i.e. $\epsilon = -1.2$ for $\gamma = 1.8$), the clustering is constant for comoving coordinates (comoving clustering), which means that the amplitude of the correlation function remains fixed with redshift in comoving coordinates as the galaxy pair expands together with the Universal expansion. Alternatively, in the $\epsilon = -3$ model the clustering is constant for physical coordinates, while $\epsilon = 0$ reflects the *stable* clustering model (e.g. de Zotti et al. 1990).

We can relate the amplitude θ_0 in two dimensions to the corresponding three-dimensional one, r_0, using Limber's integral equation (cf. Peebles 1993). For example, in the case of a spatially flat

Table 1. Angular correlation function analysis results. The columns are X-ray subsample, number of objects in the subsample, the corresponding angular correlation length, the reduced χ^2, the χ^2 probabilities and the correlation signal between 0 and 150 arcsec. The errors represent 1σ uncertainties.

X-ray band	No. of sources	θ_0 (arcsec)	χ^2/d.o.f.	P_{χ^2}	$w(\theta < 150$ arcsec)
0.5–8 keV	462	10.8 ± 1.7	1.50	0.10	0.114 ± 0.037
0.5–2 keV	432	10.4 ± 1.9	1.10	0.35	0.105 ± 0.035

Universe, Limber equation can be written as

$$w(\theta) = 2\frac{\int_0^\infty \int_0^\infty x^4\phi^2(x)\xi(r,z)\,\mathrm{d}x\,\mathrm{d}u}{\left[\int_0^\infty x^2\phi(x)\,\mathrm{d}x\right]^2}, \quad (6)$$

where $\phi(x)$ is the selection function (the probability that a source at a distance x is detected in the survey) and x is the proper distance related to the redshift through

$$x(z) = \frac{c}{H_0}\int_0^z \frac{\mathrm{d}t}{E(t)}, \quad (7)$$

with

$$E(z) = \left[\Omega_\mathrm{m}(1+z)^3 + \Omega_\Lambda\right]^{1/2} \quad (8)$$

(see Peebles 1993). The number of objects in the given survey with a solid angle Ω_s and within the shell $(z, z+\mathrm{d}z)$ is

$$\frac{\mathrm{d}N}{\mathrm{d}z} = \Omega_s x^2\phi(x)\left(\frac{c}{H_0}\right)E^{-1}(z). \quad (9)$$

Therefore, combining the above system of equations, the expression for $w(\theta)$ satisfies the form

$$w(\theta) = 2\frac{H_0}{c}\int_0^\infty \left(\frac{1}{N}\frac{\mathrm{d}N}{\mathrm{d}z}\right)^2 E(z)\,\mathrm{d}z \int_0^\infty \xi(r,z)\,\mathrm{d}u. \quad (10)$$

Note that, the physical separation between two sources, separated by an angle θ considering the small angle approximation, is given by

$$r \simeq \frac{1}{(1+z)}(u^2 + x^2\theta^2)^{1/2}. \quad (11)$$

Using equations (5) and (10) we obtain

$$\theta_0^{\gamma-1} = H_\gamma\left(\frac{r_0^\gamma H_\circ}{c}\right)\int_0^\infty \left(\frac{1}{N}\frac{\mathrm{d}N}{\mathrm{d}z}\right)^2 \frac{E(z)(1+z)^{-3-\epsilon+\gamma}}{x^{\gamma-1}(z)}\,\mathrm{d}z, \quad (12)$$

where $H_\gamma = \Gamma(1/2)\Gamma[(\gamma-1)/2]/\Gamma(\gamma/2)$.

To perform the inversion we still need to determine the source redshift distribution $\mathrm{d}N/\mathrm{d}z$. As we have no unbiased redshift information for our sources we can resort to a measure of $\mathrm{d}N/\mathrm{d}z$ using an estimate of their luminosity function. In flux-limited samples, there is a degradation of sampling as a function of distance from the observer (codified by the so-called *selection function*). The latter also depends on the evolution of the source luminosity function but is independent of the cosmological model, used in the derivation of the luminosity function. Thus, for our X-ray sources the selection function can be written as

$$\phi(x) = \int_{L_{\min}(z)}^\infty \Phi(L_x, z)\,\mathrm{d}L, \quad (13)$$

where $\Phi(L_x, z)$ is their redshift-dependent luminosity function. In this work we used the soft band luminosity functions of Miyaji, Hasinger & Schmidt (2000) and of Boyle et al. (1993). We also use different models for the evolution of the soft X-ray sources: a pure luminosity evolution (PLE) or the more realistic LDDE (Miyaji et al. 2000). In Fig. 3 we present the expected redshift distributions of the soft X-ray sources for three different luminosity functions and evolution models. The LDDE model predicts a redshift distribution shifted to much larger redshifts with a median redshift of $\bar{z} \simeq 1.2$ (see also Table 2) comparing with both the Boyle et al. (1993) and the Miyaji et al. (2000) luminosity functions with PLE. It is very interesting that the source redshift distribution of the *ROSAT* Lochman Deep field (Schmidt et al. 1998), albeit having a flux limit slightly lower than of our survey, traces quite well the LDDE predictions (see the histogram in Fig. 3), a fact that supports this luminosity function evolutionary model. To quantify this claim we have performed a χ^2 test between the observed and theoretical redshift distributions and found that the probability of consistency is 0.45 (χ^2/df = 0.97), $<10^{-6}$(χ^2/df = 8.5) and 0.04 (χ^2/df = 2.1) for the LDDE, PLE (Miyaji) and the PLE (Boyle) models, respectively.

4.2 Results

Using equation (12), the LDDE luminosity evolution model and $\epsilon = -1.2$ we find within the concordance cosmological model a soft band correlation length of $r_0 \simeq 16.4 \pm 1.3\ h^{-1}$ Mpc. This value is comparable to that of extremely red objects (EROs), luminous radio sources (Roche, Dunlop & Almaini 2003; Overzier et al. 2003; Röttgering et al. 2003) and hard X-ray sources (Basilakos et al. 2004) which are found to be in the range $r_0 \simeq 12$–$19\ h^{-1}$ Mpc. It is interesting to mention that radio sources which contain an AGN also show strong clustering ($r_0 \simeq 11\ h^{-1}$ Mpc), while the opposite is true for the case of radio sources showing no AGN activity (Magliocchetti et al. 2004).

However, our previously derived r_0 value is significantly larger than those derived from optical AGN surveys: $r_0 \simeq 5.4$–$8.6\ h^{-1}$ Mpc (Croom & Shanks 1996; La Franca, Andreani & Cristiani 1998; Akylas et al. 2000; Croom et al. 2002; Grazian et al.

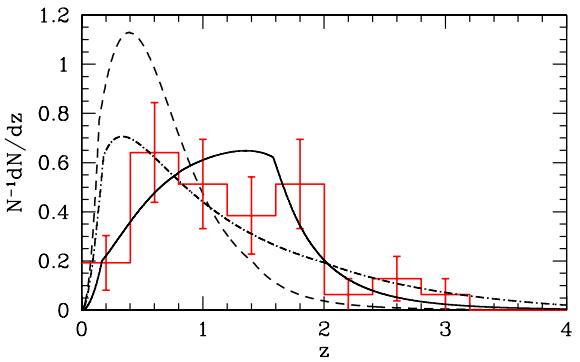

Figure 3. The redshift selection function for three different luminosity function models: (a) Miyaji et al. (2000) with PLE (dashed line), (b) Miyaji et al. (2000) with LDDE (continuous line) and (c) Boyle et al. (1993) with PLE (dot-dashed line). The histogram corresponds to the distribution of the Schmidt et al. (1998) X-ray sources of the *ROSAT* Lochman Deep Field.

Table 2. The soft X-ray sources correlation length (r_0 in h^{-1} Mpc) for different clustering models (ϵ) and for the different luminosity functions and evolution models. The right-hand column indicates the predicted median redshift, from the specific luminosity function used. The bold letters delineate the preferred cosmological model and the most updated luminosity function.

LF	Evol. model	$(\Omega_m, \Omega_\Lambda)$	r_0 ($\epsilon = -1.2$)	r_0 ($\epsilon = -3$)	$\bar{z}$
Boyle	No evol.	(1,0)	7.9 ± 0.6	5.4 ± 0.4	0.50
Miyaji	No evol.	(1,0)	6.5 ± 0.5	4.9 ± 0.4	0.37
Boyle	PLE	(1,0)	12.0 ± 1.0	6.3 ± 0.5	0.92
Miyaji	PLE	(1,0)	8.8 ± 0.7	5.7 ± 0.4	0.58
Miyaji	**LDDE**	**(0.3,0.7)**	$\mathbf{16.4 \pm 1.3}$	$\mathbf{7.5 \pm 0.6}$	**1.19**
Miyaji	LDDE	(1,0)	11.2 ± 0.9	5.0 ± 0.4	1.19

2004) as well as from the recent X-ray selected sample of Mullis et al. (2004) who find $r_0 \simeq 7.4\,h^{-1}$ Mpc. We can push our inverted r_0 values to approximate closely the latter results only if we use the clustering evolution model which remains constant for physical coordinates ($\epsilon = -3$), in which case we obtain $r_0 \simeq 7.5 \pm 0.6$ h^{-1} Mpc, and this is in excellent agreement with the results of Mullis et al. (2004). Note that earlier *ROSAT* soft X-ray clustering results of Carrera et al. (1998) found a weaker clustering, with their upper limit of the linear clustering evolution model being marginally consistent with our $\epsilon = -3$ results.

In Table 2, we list the values of the correlation length, r_0, resulting from Limber's inversion for different luminosity function, evolution models as well as for different cosmological models. We can attempt to disentangle the different sources of the apparent r_0 differences. First, comparing the LDDE model between the Einstein de Sitter (EdS) and the concordance ($\Omega_{\rm m} = 1 - \Omega_\Lambda = 0.3$) cosmological models it becomes evident that the effect of moving from the former to the latter model increases by $\sim$50 per cent the value of r_0 (for both ϵ cases). Note also that within the EdS cosmological model moving from the LDDE to the PLE luminosity evolution models decreases the value of r_0 by $\sim$20 per cent for $\epsilon = -1.2$, while for the $\epsilon = -3$ case there is no significant difference between the two luminosity evolution models. Therefore, although we do not have the PLE luminosity model parameters for the concordance cosmological model we may expect similar changes as before, which implies that within this cosmological and luminosity evolution (PLE) models we would obtain $r_0 \sim 12.5$ and $7\,h^{-1}$ Mpc for the $\epsilon = -1.2$ and $\epsilon = -3$ models, respectively.

Note also that the change of the luminosity function model and thus of the redshift selection function, is always accompanied by a change in the median redshift of the corresponding redshift distribution.

We can attempt to parametrize the different luminosity model effects on the determination of r_0 by investigating its dependence on the median redshift of the source distribution as well as on the cosmological model. To do so we use a parametrized, by the characteristic redshift $\bar{z}$, analytical selection function given by Baugh (1996)

$$\frac{{\rm d}N}{{\rm d}z} \propto z^2 \exp\left[-\left(\frac{z}{z_c}\right)^{3/2}\right], \qquad (14)$$

where $\bar{z} = \sqrt{2} z_c$ is the median redshift. Although this formula has been derived from the distribution of optical galaxies while the redshift distribution of X-ray sources may be different we find that at least the Miyaji et al. (2000) luminosity function provides absolutely consistent results. For example, on inserting equation (14) in equation (12) with $\bar{z} \simeq 1.19$ and $\epsilon = -1.2$ we find for

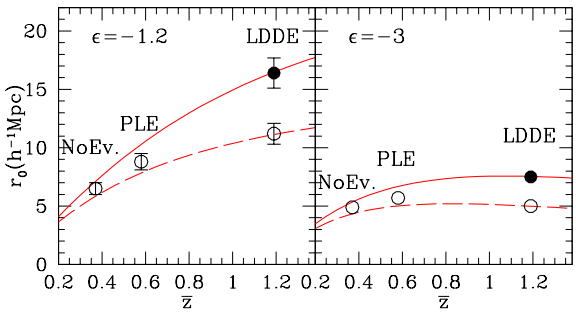

Figure 4. Comparison of the expected increase of r_0 as a function of the median redshift of the source redshift distribution for a concordance (continuous line) and an EdS model, respectively, using the parametric selection function model of Baugh (1996). The results of Table 2 based on the Miyaji et al. (2000) luminosity functions are plotted (filled circles for the concordance model and open for the EdS model).

the LDDE model $r_0 \simeq 16.3 \pm 2.0$ and $r_0 \simeq 11.0 \pm 1.5$ h^{-1} Mpc for the concordance and EdS models, respectively, which are in excellent agreement with the direct LDDE results (see Table 2). A similar level of consistency is also found for the other models presented in Table 2 (except for the models based on Boyle's luminosity function which is owing to their significant contributions from very large redshifts). In Fig. 4, we show the dependence of the derived r_0 value on the median redshift of the source distribution for the two different cosmologies and two clustering evolution models. We also plot our direct results (using the different Miyaji et al. luminosity function models that provide different $\bar{z}$ values) of Table 2. The excellent consistency is evident which makes us confident of our results. Guided by Fig. 4 we can deduce that the PLE model of the luminosity function of Miyaji et al. (2000) would provide $r_0 \simeq 12$ and $7\,h^{-1}$ Mpc within the concordance cosmological model for the $\epsilon = -1.2$ and $\epsilon = -3$ clustering models, respectively.

5 THE *XMM* SOURCES COSMOLOGICAL BIAS

Within the framework of linear biasing (cf. Kaiser 1984; Benson et al. 2000), the mass-tracer and dark-matter spatial correlations, at some redshift z, are related by

$$\xi(r, z) = \xi_{\rm DM}(r, z) b^2(z), \qquad (15)$$

where $b(z)$ is the bias evolution function.

We can quantify the evolution of clustering with epoch presenting the spatial correlation function of the mass $\xi_{\rm DM}(r, z)$ as the Fourier transform of the spatial power spectrum $P(k)$

$$\xi_{\rm DM}(r, z) = (1+z)^{-(3+\epsilon)} \frac{1}{2\pi^2} \int_0^\infty k^2 P(k) \frac{\sin(kr)}{kr}\, {\rm d}k, \qquad (16)$$

where k is the comoving wavenumber. Furthermore, the predicted spatial correlation function of the X-ray sources can be written as

$$\xi(r, z) = \frac{R(z)}{2\pi^2} \int_0^\infty k^2 P(k) \frac{\sin(kr)}{kr}\, {\rm d}k, \qquad (17)$$

where

$$R(z) = (1+z)^{-(3+\epsilon)} b^2(z). \qquad (18)$$

As for the power spectrum of our CDM models, we use $P(k) \approx k^n T^2(k)$ with scale-invariant ($n = 1$) primeval inflationary fluctuations and $T(k)$ the CDM transfer function. In particular, we use the transfer function parametrization as in Bardeen et al. (1986), with

the corrections given approximately by Sugiyama (1995). Note that we also use the non-linear corrections introduced by Peacock & Dodds (1994).

5.1 Bias evolution

The concept of biasing between different classes of extragalactic objects and the background matter distribution was put forward by Kaiser (1984) and Bardeen et al. (1986) to explain the higher amplitude of the two-point correlation function of clusters of galaxies with respect to that of galaxies themselves.

The deterministic and linear nature of biasing has been challenged (cf. Bagla 1998; Dekel & Lahav 1999) and indeed on small scales ($r < 10\,h^{-1}$ Mpc) there are significant deviations from $b(r) = \text{const}$. Despite this, the linear biasing assumption is still a useful first-order approximation which, owing to its simplicity, is used in most studies of large-scale clustering (cf. Magliocchetti et al. 1999). In this paper, however, we will work within the paradigm of linear and scale-independent bias. A number of bias evolution models have been proposed based on different assumptions (e.g. Nusser & Davis 1994; Fry 1996; Mo & White 1996; Matarrese et al. 1997; Tegmark & Peebles 1998; Bagla 1998; Basilakos & Plionis 2001). However, here we will discuss two that have been shown to describe relatively well the evolution even beyond $z \sim 1$.

(i) *Merging Bias Model* (hereafter B2): Mo & White (1996) have developed a model for the evolution of the the so-called correlation bias, using the Press–Schechter formalism. Utilizing a similar formalism, Matarrese et al. (1997) extended the Mo & White (1996) results to include the effects of different mass scales (see also Moscardini et al. 1998; Bagla 1998; Catelan et al. 1998; Magliocchetti et al. 1999). In this case we have

$$b_{\rm B2}(z) = 0.41 + \frac{(b_0 - 0.41)}{D^{\beta}(z)}, \tag{19}$$

with $\beta \simeq 1.8$. Note that $D(z)$ is the linear growth rate of clustering (cf. Peebles 1993)[1] scaled to unity at the present time.

(ii) *Bias from Linear Perturbation Theory* (hereafter B3): Basilakos & Plionis (2001, 2003), using linear perturbation theory and the Friedmann–Lemaitre solutions of the cosmological field equations have derived analytically the functional form for the evolution of the linear bias factor, b, between the background matter and a mass-tracer fluctuation field. For the case of a spatially flat Λ cosmological model ($\Omega_{\rm m} + \Omega_{\Lambda} = 1$), the bias evolution can be written as

$$b_{\rm B3}(z) = \mathcal{A}E(z) + \mathcal{C}E(z)K(z) + 1 \tag{20}$$

with

$$K(z) = \int_{1+z}^{\infty} \frac{y^3}{[\Omega_{\rm m} y^3 + \Omega_{\Lambda}]^{3/2}}\,{\rm d}y \tag{21}$$

or

$$K(z) = (1+z)^{-1/2} F\left[\frac{1}{6}, \frac{3}{2}, \frac{7}{6}, -\frac{\Omega_{\Lambda}}{\Omega_{\rm m}(1+z)^3}\right], \tag{22}$$

where F is the hyper-geometric function. Note that this approach gives a family of bias curves, owing to the fact that it has two unknown parameters (the integration constants $\mathcal{A}, \mathcal{C}$). Basilakos & Plionis (2001, 2003) compared the B3 bias evolution model with other models as well as with the HDF (*Hubble Deep Field*) biasing results Magliocchetti et al. (1999); Arnouts et al. (2002), and found a very good consistency. In this work, for simplicity, we fix the value of $\mathcal{C}$ being $\simeq$0.004, as was determined in Basilakos & Plionis (2003) from the 2dF galaxy correlation function. It is evident that the bias factor at the present time can be obtained from equation (20) for $z = 0$

$$b_{\rm B3}(0) = \mathcal{A} + \mathcal{C}K(0) + 1, \tag{23}$$

where we have used $E(0) = 1$. Note that $K(0) \simeq 9.567$ for $\Omega_{\Lambda} = 1 - \Omega_{\rm m} = 0.7$.

5.2 The bias at the present time b_0

Based on the LDDE (Miyaji et al. 2000) we quantify the bias factor at the present time b_0, performing a standard χ^2 minimization procedure between the measured correlation function for the soft band 0.5–2 keV with that expected in our ΛCDM cosmological model

$$\chi^2(b_0) = \sum_{i=1}^{n} \left[\frac{w_{\rm XMM}(\theta^i) - w_{\rm model}\left(\theta^i, b_0\right)}{\sigma^i}\right]^2, \tag{24}$$

where σ^i is the observed $w(\theta)$ uncertainty.

In Fig. 5 we present for the two bias and clustering evolution models the variation of $\Delta\chi^2 = \chi^2(b_0) - \chi^2_{\rm min}(b_0)$ around the best b_0 fit, while in Table 3 we list the results of the corresponding fits for all the models under consideration. The resulting present time bias is between $b_0 \simeq 1.05$–1.90 and $b_0 \simeq 1.64$–2.74 for the B2 and B3 bias models, respectively. Note that the theoretical (ΛCDM + B3 bias model) fit to the measured soft X-ray source angular correlation function is presented as the solid line in Fig. 2.

To understand better the effects of AGN clustering, we present in Fig. 6 the quantity $R(z)$ (see equation 18) as a function of redshift for the concordance cosmological model and for different bias evolution models. It is quite obvious that the behaviour of the function $R(z)$ characterizes the clustering evolution with epoch; in general AGN clustering is a monotonically increasing function of redshift for both B2 and B3 biasing models. Fig. 6, for example, clearly shows that the bias at high redshifts has different values in the different clustering models. In particular, for the comoving clustering, $\epsilon = -1.2$ (continuous line for B3 and filled points for B2), the distribution of soft X-ray sources is strongly biased ($1.90 \lesssim b_0 \lesssim 2.74$), as opposed to the less biased distribution ($1.05 \lesssim b_0 \lesssim 1.64$) in the $\epsilon = -3$ (dashed line for B3 and crosses for B2) clustering model. This is to be expected, simply because the value $\epsilon = -3$ removes the $(1 + z)$ dependence from the $R(z)$ functional form and thus,

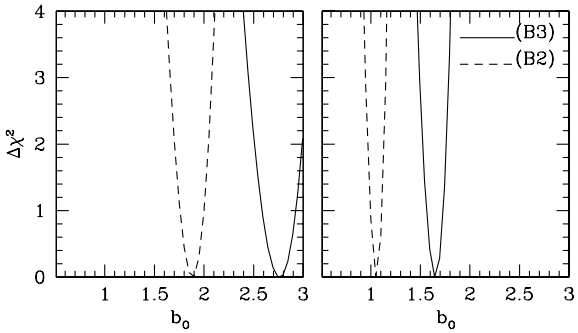

Figure 5. The variation of $\Delta\chi^2$ around the best bias fit (b_0) using different clustering behaviours (left-hand panel for $\epsilon = -1.2$ and right-hand panel for $\epsilon = -3$). Note that the solid and dashed lines represent the bias from the linear perturbation (B3) and the merging (B2) bias models, respectively.

[1] $D(z) = (1+z)^{-1}$ for an EdS universe.

Table 3. Results of the predicted soft X-ray sources bias. The correspondence of the columns is as follows: bias and clustering evolution models, b_0 is the bias at the present time, the reduced χ^2 and the χ^2 probabilities. Errors of the fitted parameters represent 1σ uncertainties.

Bias model	ϵ	b_0	χ^2/d.o.f.	P_{χ^2}
B2	-1.2	1.90 ± 0.10	0.97	0.49
B3	-1.2	2.74 ± 0.15	0.86	0.60
B2	-3.0	1.05 ± 0.05	0.97	0.49
B3	-3.0	1.64 ± 0.05	0.84	0.63

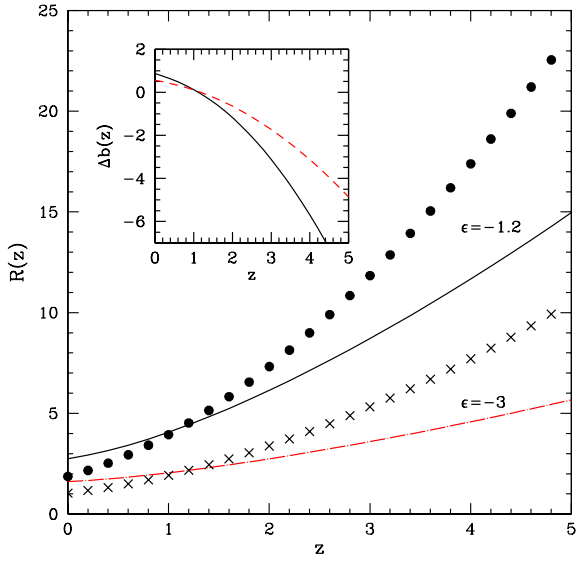

Figure 6. The function $R(z) = (1+z)^{-(3+\epsilon)} b^2(z)$ as a function of redshift. The continuous line (B3 bias) and the filled point (B2 bias) types represent the $R(z)$ behaviour in the framework of a comoving clustering ($\epsilon = -1.2$), while the dot-dashed line (B3 bias) and the crosses (B2 bias) are based on a clustering model which is constant for physical coordinates ($\epsilon = -3$). In the insert we present the difference, $\Delta b(z) = b_{\rm B3}(z) - b_{\rm B2}(z)$, between the (B3) and (B2) bias models as a function of z for $\epsilon = -1.2$ (continuous line) and $\epsilon = -3$ (dashed line), respectively.

produces a lower corresponding correlation length (see Table 2), in contrast with the comoving ($\epsilon = -1.2$) clustering case. In other words, the higher or lower correlation length corresponds to a higher or lower bias at the present time, respectively, being consistent with the hierarchical clustering scenario (cf. Magliocchetti et al. 1999). Note, that the above predictions are in good agreement with those derived by Treyer et al. (1998), Carrera et al. (1998), Barcons et al. (2000) and Boughn & Crittenden (2004), who found that $b_0 \sim 1$–2.

With respects to the predictions of the two bias models, we present in the insert of Fig. 6 the difference, $\Delta b(z) = b_{\rm B3}(z) - b_{\rm B2}(z)$, between the B3 bias model and the Matarrese et al. (1997) model B2 as a function of redshift. The B2 bias evolves significantly more than the B3 model at relatively low redshifts ($z \leqslant 1.0$), which could be attributed to our assumption that the galaxy number density is conserved in time. It is evident that merging processes, not taken into account in the B3 model, are probably important in the evolution of clustering.

It is evident that the behaviour of the inverted X-ray source spatial correlation function is sensitive to the different values of ϵ but there is also a strong dependence on the bias models that we have considered in our analysis. We can attempt to select the most viable bias and the clustering evolution models by the following.

(i) Invoking the results of the local X-ray AGN clustering of Akylas et al. (2000) and Mullis et al. (2004), who find $r_0 \simeq 6.5$ and 7.4 h^{-1} Mpc, respectively.

(ii) Noting that the local galaxy distribution, with a correlation length $r_0 \simeq 5\ h^{-1}$ Mpc, is unbiased with respect to the corresponding underline matter distribution (e.g. Lahav et al. 2002; Verde et al. 2002).

These two facts leads us to a local bias between the X-ray selected AGN population and the underline matter distribution of

$$b(0) = (r_{\circ,\rm m}/r_{\circ,\rm AGN})^{-0.9} \sim (5/7)^{-0.9} \simeq 1.35\ ,$$

which is consistent only with the $\epsilon = -3$ model of clustering evolution while it is in between the predictions of the two bias models used.

6 CONCLUSIONS

We have studied the angular clustering properties of the soft (0.5–e keV) X-ray point sources found in the *XMM–Newton*/2dF survey. We find that there is a strong (3σ) clustering signal. Indeed, if the two-point angular correlation function is modelled as a power law, $w(\theta) = (\theta_0/\theta)^{0.8}$, then after correcting for the integral constraint and the amplification bias the best-fitting angular clustering length is $\theta_0 \simeq 10.4 \pm 1.9$ arcsec.

Inverting Limber's equation and using the preferred luminosity dependent density evolution model for the luminosity function gives $r_0 \simeq 16$ and 7.5 h^{-1} Mpc, for the clustering evolution models that are constant for comoving ($\epsilon = -1.2$) and in physical ($\epsilon = -3$) coordinates, respectively. In the former case, the values for the clustering length are comparable with those of EROs and luminous radio sources, and are significantly higher than those found from previous *ROSAT* surveys (e.g. Vikhlinin & Forman 1995; Carrera et al. 1998; Akylas et al. 2000; Mullis et al. 2004) and optical QSO surveys such as the 2QZ (Croom et al. 2002) and that of Grazian et al. (2004). However, we obtain quite a good agreement with the above surveys only in the case of a clustering evolution model where the clustering length remains constant for physical coordinates ($\epsilon = -3$).

Comparing the measured angular correlation function for the soft band 0.5–2 keV X-ray sources with the theoretical predictions of the preferred ΛCDM cosmological model ($\Omega_{\rm m} = 1 - \Omega_\Lambda = 0.3$) and two bias evolution models, we find that the present bias values is in the range of $1.9 \lesssim b_0 \lesssim 2.7$ for the $\epsilon = -1.2$ model and $1.0 \lesssim b_0 \lesssim 1.6$ for the $\epsilon = -3$ model.

ACKNOWLEDGMENTS

SB acknowledges the hospitality of the Astrophysics Department of INAOE where this work was completed. The ΛCDM simulation used in this paper was carried out by the Virgo Supercomputing Consortium using computers based at the Computing Centre of the Max-Planck Society in Garching and at the Edinburgh parallel Computing Centre. The data are publicly available at http://www.mpa-garching.mpg.de/NumCos. We thank the referee, F. Carrera, for useful suggestions.

This work is jointly funded by the European Union and the Greek Government in the framework of the programme 'Promotion of Excellence in Technological Development and Research', project 'X-ray Astrophysics with ESA's mission *XMM*'. Furthermore, MP

acknowledges support by the Mexican Government through Grant No. CONACyT-2002-C01-39679.

REFERENCES

Akylas A., Georgantopoulos I., Plionis M., 2000, MNRAS, 318, 1036
Arnouts S. et al., 2002, MNRAS, 329, 355
Bagla J. S., 1998, MNRAS, 417, 424
Baldi A., Molendi S., Comastri A., Fiore F., Matt G., Vignali C., 2002, ApJ, 564, 190
Barcons X., Carrera F. J., Ceballos M. T., Mateos S., 2000, in White N. et al., eds, X-ray Astronomy 99: Stellar Endpoints, AGN and the Diffuse X-ray Background, AIP Conference Proceedings 599, p. 3 (astro-ph/0001182)
Bardeen J. M., Bond J. R., Kaiser N., Szalay A. S., 1986, ApJ, 304, 15
Basilakos S., 2001, MNRAS, 326, 203
Basilakos S., Plionis M., 2001, ApJ, 550, 522
Basilakos S., Plionis M., 2003, ApJ, 593, L61
Basilakos S., Georgakakis A., Plionis M., Georgantopoulos I., 2004, ApJL, 607, L79
Baugh C. M., 1996, MNRAS, 280, 267
Benson A. J., Cole S., Frenk S. C., Baugh M. C., Lacey G. C., 2000, MNRAS, 311, 793
Boughn S. P., Crittenden R. G., 2004, ApJ, 612, 647
Boyle B. J., Mo H. J., 1993, MNRAS, 260, 925
Boyle B. J., Griffiths R. E., Shanks T., Stewart G. C., Georgantopoulos I., 1993, MNRAS, 260, 49
Carrera F. J., Barcons X., Fabian A. C., Hasinger G., Mason K. O., McMahon R. G., Mittaz J. P. D., Page M. J., 1998, MNRAS, 299, 229
Catelan P., Lucchin F., Matarese S., Porciani C., 1998, MNRAS, 297, 692
Croom S. M., Shanks T., 1996, MNRAS, 281, 893
Croom S. M., Shanks T., Boyle B. J., 2001, MNRAS, 325, 483
Croom S. M., Boyle B. J., Loaring N. S., Miller L., Outram P. J., Shanks T., Smith R. J., 2002, MNRAS, 335, 459
Dekel A., Lahav O., 1999, ApJ, 520, 24
de Zotti G., Persic M., Franceschini A., Danese L., Palumbo G. G. C., Boldt E. A., Marshall F. E., 1990, ApJ, 351, 22
Efstathiou G., Bernstein G., Katz N., Tyson J. A., Guhathakurta P., 1991, ApJ, 380, L47
Freedman W. L. et al., 2001, ApJ, 553, 47
Frenk C. S. et al., 2000, astro-ph:0007362
Fry J. N., 1996, ApJ, 461, 65
Georgakakis A., Georgantopoulos I., Stewart G. C., Shanks T., Boyle B. J., 2003, MNRAS, 344, 161
Georgakakis A. et al., 2004, MNRAS, 349, 135
Georgantopoulos I., Stewart G. C., Shanks T., Boyle B. J., Griffiths R. E., 1996, MNRAS, 280, 276
Grazian A., Negrello M., Moscardini L., Cristiani S., Haehnelt M. G., Matarese S., Omizzolo A., Vanella E., 2004, AJ, 127, 592
Kaiser N., 1984, ApJ, 284, L9
Kirkman D., Tytler D., Suzuki N., O'Meara J. M., Lubin D., 2003, ApJS, 149, 1
La Franca F., Andreani P., Cristiani S., 1998, ApJ, 497, 529
Lahav O. et al., 2002, MNRAS, 333, 961
Magliocchetti M., Maddox S. J., Lahav O., Wall J. V., 1999, MNRAS, 306, 943
Magliocchetti M. et al., 2004, MNRAS, 350, 148
Manners J. C. et al., 2003, MNRAS, 343, 293
Mason K. O. et al., 2000, MNRAS, 311, 456
Matarrese S., Coles P., Lucchin F., Moscardini L., 1997, MNRAS, 286, 115
Miyaji T., Hasinger G., Schmidt M., 2000, A&A, 353, 25
Mo H. J., White S. D. M., 1996, MNRAS, 282, 347
Moscardini L., Coles P., Lucchin F., Matarrese S., 1998, MNRAS, 299, 95
Mullis C. R., Henry J. P., Gioia I. M., Böhringer H., Briel U. G., Voges W., Huchra J. P., 2004, ApJ, in press (astro-ph/0408304)
Nusser A., Davis M., 1994, ApJ, 421, L1
Olive K. A., Steigman G., Walker T. P., 2000, Phys. Rep., 333, 389
Overzier R. A., Röttgering H., Rengelink R. B., Wilman R. J., 2003, A&A, 405, 53
Peacock A. J., Dodds S. J., 1994, MNRAS, 267, 1020
Peebles P. J. E., 1993, Principles of Physical Cosmology. Princeton University Press, Princeton, NJ
Peebles P. J. E., Ratra B., 2003, RvMP, 75, 559
Roche N. D., Dunlop J., Almaini O., 2003, MNRAS, 346, 803
Röttgering H., Daddi E., Overzier R. A., Wilman R. J., 2003, New Astron. Rev., 47, 309
Schmidt M. et al., 1998, A&A, 329, 495
Soneira R. M., Peebles P. J. E., 1978, AJ, 83, 845
Spergel D. N. et al., 2003, ApJs, 148, 175
Sugiyama N., 1995, ApJS, 100, 281
Tegmark M., Peebles P. J. E., 1998, ApJL, 500, L79
Tegmark M. et al., 2004, PhRvD, 69, 3501
Treyer M., Scharf C., Lahav O., Jahoda K., Boldt E., Piran T., 1998, ApJ, 509, 531
Verde L. et al., 2002, MNRAS, 335, 432
Vikhlinin A., Forman W., 1995, ApJ, 455, 109
Woods D., Fahlman G. G., 1997, ApJ, 490, 11
Yang Y., Mushotzky R. F., Barger A. J., Cowie L. L., Sanders D. B., Steffen A. T., 2003, ApJ, 585, L85

This paper has been typeset from a TEX/LATEX file prepared by the author.